Cellulose Fast Pyrolysis Activated by Intramolecular Hydrogen Bonds

Fuat Sakirler and Hsi-Wu Wong*

Department of Chemical Engineering, University of Massachusetts Lowell, One University Avenue, Lowell, Massachusetts 01854, United States

Corresponding Author

*E-mail: hsiwu_wong@uml.edu. Tel.: 1-978-934-5290.

ORCID

Hsi-Wu Wong: 0000-0003-2623-6145

Fuat Sakirler: 0000-0001-5144-0469

Abstract

The conversion of inedible biomass by fast pyrolysis is a promising route for sustainable production of renewable fuels and value-added chemicals, but low selectivity towards desired products hampers its economic viability. Understanding the molecular-level reaction pathways of biomass fast pyrolysis could be the key to overcome this challenge. However, the effects of intramolecular and interchain hydrogen bonds near the reaction center have not been thoroughly explored. In this work, reaction pathways and kinetics of fast pyrolysis of cellulose, the major component of biomass, were investigated using density functional theory. A new intramolecular hydroxyl-activated mechanism is presented for cellulose activation. Our calculations incorporating noncovalent interactions accurately captured the activation energy of 50.8 kcal mol^{-1}, agreeable with the apparent activation energy measured experimentally. The findings of cellulose pyrolysis provide insights into the investigation of interactions during real-life biomass pyrolysis.

Keywords: biomass, cellulose pyrolysis, density functional theory calculations, hydrogen bond interactions, reaction mechanism.

1. Introduction

Rapid consumption of fossil-derived fuels has caused increased concerns over sustainability and climate change.[1] Using renewable energy is a viable option to meet the ever-increasing energy demands.[2] Among the available renewable energy sources, lignocellulosic (non-edible) biomass is an abundant and widely available carbon-neutral feedstock that can be converted into biofuels for feasible energy storage. As a result, biomass conversion methods have attracted significant attention over the last decade.[3]

Currently, both thermochemical and biochemical methods are being explored for the conversion of lignocellulosic biomass.[4] Thermochemical methods such as gasification, pyrolysis, and hydrothermal liquefaction have the benefits of simplicity and similarity to the existing petrochemical operations. In particular, biomass fast pyrolysis, which transforms the feedstocks into biofuels or value-added chemicals in the absence of oxygen at elevated temperatures (400–1000 °C),[5] has drawn extensive interest.[6] Since biomass fast pyrolysis occurs at a very short timescale, approximately a few seconds,[5] obtaining the molecular-level kinetic information *via* experiments is typically challenging.[7] Consequently, in-depth understanding of biomass pyrolysis chemistry using quantum chemistry (QC) plays a key role to the advancement of the biomass fast pyrolysis technologies.[8]

Cellulose is the most abundant constituent of lignocellulosic biomass and is widely distributed in nature. The major pyrolytic products from cellulose pyrolysis includes various anhydrosugars as well as smaller C_1 to C_5 low-molecular-weight products.[9-11] Levoglucosan (LG, 1,6-anhydro-β-D-glucopyranose) is the most abundant product from cellulose fast pyrolysis.[12] Many theoretical studies over the last decade have been dedicated to the revelation of molecular-level reaction pathways of LG formation from cellulose pyrolysis.[13] Since cellulose bears long linear chains of homopolymer of β-D-glucopyranose monomers linked by β-1,4 glycosidic bonds, the scission of the glycosidic bonds is the key reaction during fast pyrolysis. Three different mechanisms of glycosidic bond cleavage have been proposed, namely homolysis, heterolysis, and concerted mechanism. It was reported that the concerted mechanism[14-16] has the lowest activation barrier in the range of 46–60 kcal mol^{-1} in comparison to homolysis[17-19] and heterolysis.[18-20] This concerted mechanism

involves simultaneous cleavage of the glycosidic C-O bond and formation of a bicyclic ring *via* connecting the electrophile carbon and oxygen atoms of the hydroxymethyl group, which converts a cellulose polymer chain into shorter anhydro-oligosaccharides terminated with LG, called "active cellulose".[21, 22] Experimental studies reported the presence of "active cellulose" with degrees of polymerization in the range of 2–10.[23] These anhydro-oligosaccharides can then undergo successive concerted cleavage of the end-unit glycosidic bonds to produce LG.

The elementary reaction pathways of cellulose pyrolysis have been widely investigated experimentally[24-26] and theoretically.[27-29] Although concerted glycosidic bond cleavage is generally accepted as the most likely mechanism,[14, 30] the molecular picture describing the effects of the vicinity of the reaction center during cellulose pyrolysis is less studied. Seshadri and Westmoreland[31] performed density functional theory (DFT) calculations on β-D-glucose to show that glycosidic bond cleavage could be catalyzed *via* vicinal hydroxyl groups from nearby cellulose polymers or pyrolysis products such as water and other hydroxylated solvents. Maliekkal et al.[29] suggest that the glycosidic bond could be catalytically activated by hydroxyl groups from neighboring cellulose sheets at low temperatures (< 467 °C). Hosoya and Sakaki[15] used two- and three-chain oligomers to demonstrate that interchain hydrogen bonds increase the activation energy of glycosidic bond cleavage, although their conclusions were drawn based on the less favorable anti conformation without allowing the pyranose rings of the chains to freely rotate and performing frequency calculations on the largest (multi-chain) model.

While the above theoretical studies suggest that hydroxyl groups near the reaction center have the potential to alter the reaction barrier of glycosidic bond cleavage, the effects of intramolecular and interchain hydrogen bonds caused by ring puckering and different orientations of ring substituents need to be further elucidated. In this work, DFT calculations were performed to elucidate the role of intramolecular hydroxyl groups near the reaction center of cellulose activation and subsequent LG formation *via* concerted glycosidic bond cleavage during cellulose pyrolysis. A new intramolecular hydroxyl-activated mechanism to facilitate concerted glycosidic bond cleavage is presented. Possible conformational pathways of glycosidic bond

cleavage are explored. The effects of intramolecular and interchain hydrogen bonds within the cellulose pyrolysis framework are determined.

2. Computational Methods

DFT calculations were performed by the Gaussian 16 package.[32] The structure optimization and frequency calculations were carried out at the meta hybrid density-functional M06-2X[33] coupled with the 6-31+G(2df,p) level of theory. The method M06-2X has been widely used for carbohydrate systems and has been reported to accurately predict reaction barriers of unimolecular reactions.[22, 34, 35] All calculations were carried out in the gas phase. Explicit or implicit solvent models were not considered in this study. The electronic effects of the environment of the reaction centers were considered by employing models of different chain lengths. Partial charges were evaluated with the CHelpG scheme.[36]

Frequency calculations were performed to verify that all saddle points have exactly one negative frequency and all minima have zero imaginary frequency. The transition state structures (TSs) were searched by the Berny algorithm[37] and synchronous transit-guided quasi-Newton method.[38] Intrinsic reaction coordinate (IRC) calculations were employed using the Hessian-based predictor-corrector integration algorithm,[39-41] and the optimization calculations on the final points of the IRC calculations were conducted to confirm that TSs connect the reactants and the products of interest. The coordinates and absolute energies of the stable structures and TSs are reported in the Supporting Information (SI).

It is well known that contributions from the vibrational motions at low frequency modes are hampered by the harmonic oscillator approximation.[42-45] In our work, the overestimation of the vibrational entropies was treated by quasi-rigid-rotor-harmonic-oscillator approach proposed by Grimme,[46] which interpolates between the harmonic vibrational and free rotor entropy. The cut-off frequency was set to 150 cm^{-1} (within the usual limits 50–150 cm^{-1}). The exponent of the Head-Gordon damping function[47] was chosen as 4 (same value used by Grimme).

For each reaction studied, the Gibbs free energy of activation, $\Delta^{\ddagger}G^{0}$, was determined from the difference between the Gibbs free energy of the TS and that of the most stable reactant. The rate constants were calculated using the transition state theory based on the Eyring-Polanyi equation[48, 49] over a temperature range of 300–1500 K with an interval of 100 K. The reported activation energy and pre-exponential factor values were obtained from the Arrhenius plot.

The structure of native cellulose has a complex hydrogen bond network with crystalline and amorphous regions. The degree of polymerization can be as high as 7,000–15,000 in native cellulose.[50] This level of complexity makes modeling the entire cellulose framework using QC impractical.[7] Consequently, small molecules such as β-D-glucose,[31] methyl β-D-glucoside,[30] cellobiose,[18] methyl-cellobiose,[14] and cellotriose[22] have been commonly used as model compounds of cellulose for studying cellulose pyrolysis with QC. In this study, three different cellulose models were constructed to investigate concerted glycosidic bond cleavage during cellulose fast pyrolysis. Methyl-cellobiose, which is cellobiose with the addition of a methyl group attached to the glycosidic oxygen of the non-reducing end, was used as the smallest structure containing a β-1,4 glycosidic bond. The non-reducing end of cellobiose was terminated with a methyl group instead of a hydrogen atom to represent the bonding environment of the glycosidic oxygen atom connecting to a neighboring unit in a cellulose chain. As recommended by Mayes and Broadbelt,[14] this treatment inhibits an unrealistic hydrogen bond at this location when a hydrogen atom is used. The methyl-cellobiose model also has the main characteristics of cellulose such as glycosidic linkage, intramolecular hydrogen bonds, and intrinsic units of both non-reducing and reducing ends. Cellotetraose was selected as the model compound to mimic a single cellulose chain. Two cellotetraose chains orientated in the same direction were used as a two-chain model to evaluate the effects of noncovalent interactions between the two chains in the same cellulose sheet during cellulose pyrolysis.

Unless otherwise noted, all calculations in the one-chain and two-chain models, including geometry optimizations and frequency calculations, were performed using a 2-layer ONIOM (Our own N-layered Integrated molecular Orbital and molecular Mechanics) method[51-53] at the M06-2X/6-31+G(2df,p):M06-

2X/6-31G(d,p) level of theory. The 2-layer ONIOM method was utilized to overcome the practical limit of computing resources. Noncovalent interactions can play an important role in calculating accurate intermolecular interaction energies of large systems.[54] Consequently, the evaluation of noncovalent interactions was mediated by the D3 version[55, 56] of dispersion-correction damping parameters in the two-chain model in our work.

The conformations of the pyranose rings in this study are described according to the IUPAC nomenclature.[57] The shapes of the six-membered rings are described by a capital letter, including chair (C), twisted-boat (S), boat (B), half-chair (H), and envelope (E).[58] Superscript and subscript before and after the capital letters denote the atoms above and below the reference plane, respectively.

The relative position of the hydroxymethyl groups defines the syn and anti conformations between the two neighboring rings along a cellulose chain, where the syn conformation indicates that the hydroxymethyl groups of the two adjacent β-D-glucopyranose units are on the opposite side and the anti conformation indicates that the hydroxymethyl groups are poised on the same side.

The crystalline structure of cellulose has a complex network consisting of intra- and inter- molecular hydrogen bonds.[59, 60] In this study, the classifications of hydrogen bonds is based on the spatial distance between a hydrogen atom and an acceptor (D-H···A) and the hydrogen bond angle between the donor, hydrogen, and the acceptor (< DHA), respectively.[61] A hydrogen bond is defined to exist if D-H···A is less than 3 Å and < DHA is greater than 90°. In addition, the strong, moderate, and weak hydrogen bonds are defined as a D-H···A of 1.2–1.5 Å, 1.5–2.2 Å, and 2.2–3.0 Å and a < DHA of 175–180°, 130–180°, and 90–150°, respectively.

3. Results and discussion

3.1. Conformational Search of Methyl-Cellobiose

Obtaining the lowest-energy structure of the reactant as well as the transition state is critical to accurately predict the energy barrier of a reaction using QC. Methyl-cellobiose was first used to probe the molecular mechanism of cellulose pyrolysis leading to "active cellulose". In the absence of crystallographic data, the starting structure for the methyl-cellobiose geometry optimization calculation was based on the crystal structure of β-cellobiose reported by Kimuara and co-workers,[62] with a methyl group attached to its non-reducing end.

The pseudorotation of the pyranose rings as well as the orientations of the ring substituents can produce numerous conformations, resulting in significant energetic differences in the Gibbs free energy (by several kcal mol^{-1}) between the different conformers of the same ring puckering.[34] In this study, the conformers of methyl-cellobiose were discovered by a conformational structure search using glycosidic torsion angles. The details of the conformational search can be found in Section S1 of SI. The scan unraveled five stable ring conformers; in particular, the $^4C_1$ (chair), $B_{O,3}$ (boat), $^3S_1$ (twisted-boat), $B_{1,4}$ (boat), and $^1C_4$ (inverted chair) conformations. Of the five ring puckering conformations, $^4C_1$ is the most stable, consistent with the observed experimental structures of native cellulose[59] and β-cellobiose.[62] Figure 1 shows the lowest-energy syn-$^4C_1$ methyl-cellobiose conformers with hydroxymethyl groups of the non-reducing end poised in the gauche-gauche (GG), trans-gauche (TG), and gauche-trans (GT) orientations.

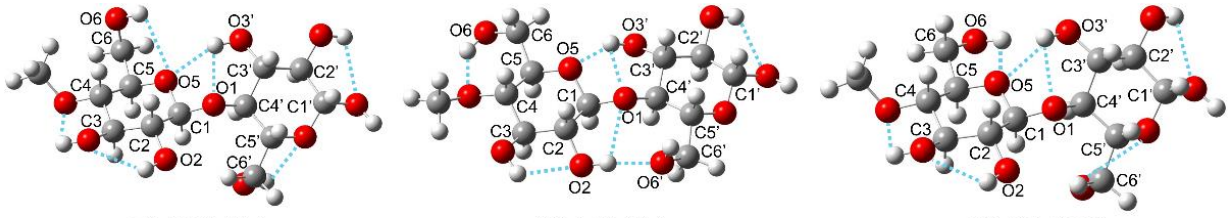

Figure 1. The calculated lowest-energy syn $^4C_1$ methyl-cellobiose conformers in the GG (**S1**), TG (**S2**), and GT (**S3**) orientations. Blue dotted lines represent hydrogen bonds.

In native cellulose, various local hydrogen bonding patterns may interchange and coexist in different positions.[59] As illustrated in Figure 1, the orientations of the hydroxymethyl groups change the pattern of hydrogen bonds at different locations. In each hydroxymethyl group orientation, the hydroxyl group at oxygen atom O3' donates a bifurcated hydrogen bond to oxygen atom O5 and glycosidic oxygen atom O1. In addition, the TG orientation (**S2**) allows a hydrogen bond between the O2 hydroxyl group and the O6' hydroxymethyl group, while no such hydrogen bond exists in the other two orientations, where the ring oxygen O5 accepts hydrogen bonds from the O6 hydroxymethyl group.

Of the above methyl-cellobiose rotamers found in the syn conformation, **S1** is the lowest-energy structure at the typical pyrolysis temperature of 773.15 K, suggesting that the hydroxymethyl group prefers the GG orientation at this temperature. This is agreeable with the molecular dynamics calculations by Matthews et al. that the hydroxymethyl groups of native cellulose can access to the GG orientation at higher temperatures (> 500 K).[63] Our calculations show that the lowest-energy structures in the TG (**S2**) and GT (**S3**) orientations have the Gibbs free energy 2.4 kcal mol^{-1} and 1.0 kcal mol^{-1} higher than that of **S1**, respectively. The structural and energetic information of several lowest-energy conformers is listed in Section S1 of SI. The energies of other local minima and TSs are given relative to **S1**.

3.2. Methyl-Cellobiose Pre-Activation *via* Ring Puckering

Previous theoretical studies[31, 34] showed that the carbohydrate pyranose rings undergo puckering before glycosidic bond cleavage. A ring puckering isomerization from syn-$^4C_1$ conformation to anti-$^1C_4$ conformation was suggested in the cellobiose model by Hosoya et al.[15, 30] However, they did not consider ring puckering from syn-$^4C_1$ conformation to syn-$^1C_4$ conformation. In this study, isomerization pathways between $^4C_1$, $B_{O,3}$, and $^1C_4$ conformations were studied using the methyl-cellobiose model. Pseudorotational ring puckering in the syn conformation taking place under cellulose pyrolysis conditions was examined. The energy barrier for the interconversion from $^4C_1$ to $B_{O,3}$ was calculated as 8.5 kcal mol^{-1}. The lowest-energy conformer in $B_{O,3}$ has a Gibbs free energy of 4.6 kcal mol^{-1} higher than **S1** in $^4C_1$. The interconversion between $B_{O,3}$ and $^1C_4$ was calculated to have an activation energy of 14.0 kcal mol^{-1}. The lowest-energy

conformer in $^{1}C_4$ has a Gibbs free energy 5.3 kcal mol^{-1} higher than **S1** in $^{4}C_1$. The calculated activation energy of both ring puckering reactions are unequivocally lower than the reported range of activation energy values of the concerted glycosidic bond cleavage (46–60 kcal mol^{-1}),[14-16] suggesting that ring puckering reactions are more rapid than glycosidic bond cleavage under pyrolysis conditions.

Section S2 of SI contains the structures of the lowest-energy ring conformers as well as TSs, rate parameters, energetics, itineraries of the isomerization reaction pathways. All ring conformations studied in this work are classified into two groups dependent on their likelihood to undergo glycosidic bond cleavage. It was determined in our calculations that only $B_{O,3}$ and $^{1}C_4$ are capable of subsequent activation *via* glycosidic bond cleavage and they are thus classified as "preactivated". Other stable preactivated conformations may exist, although our immense conformational search (Table S1 of SI) found no other conformations leading to cellulose activation. The $^{4}C_1$, $^{3}S_1$, and $B_{1,4}$ conformations were not found to lead to glycosidic bond activation in our calculations and are thus classified as "inactivated".

The structural properties of the five lowest-energy ring pucker conformations (preactivated $B_{O,3}$ and $^{1}C_4$ and inactivated $^{4}C_1$, $^{3}S_1$, and $B_{1,4}$) were analyzed to reveal the characteristics of cellulose pre-activation. The inactivated conformations are only considered as benchmarks for comparison. The mechanism of concerted glycosidic bond cleavage during cellulose pyrolysis includes the formation of an oxocarbenium ion-like TS,[15, 30] which has a double-bond character between the anomeric carbon atom C1 and ring oxygen atom O5. As a result, the elongated C1-O1 bond and the shortened C1-O5 bond are considered as indicators of an oxocarbenium ion-like structure that favors glycosidic bond cleavage.[34, 64] Figures 2a and 2b demonstrate the calculated distances of the C1-O1 and C1-O5 bonds of each lowest-energy conformation. The C1-O1 bonds of the preactivated $B_{O,3}$ and $^{1}C_4$ conformations are longer than that of the undistorted $^{4}C_1$ conformation by 0.024 and 0.033 Å, respectively. The C1-O1 bonds of the inactivated $^{4}C_1$, $^{3}S_1$, and $B_{1,4}$ conformations all remain below 1.40 Å. The C1-O5 bonds of preactivated $B_{O,3}$ and $^{1}C_4$ are shorter than that of $^{4}C_1$ by 0.012 and 0.018 Å, respectively. On the other hand, the C1-O5 bonds of inactivated $^{3}S_1$ and $B_{1,4}$ are slightly elongated by approximately 0.002 Å. Our calculations reveal that the preactivated $B_{O,3}$ and $^{1}C_4$

conformations are structurally resemblant of the oxocarbenium ion-like TS, making them the energetically and structurally favorable conformations to undergo subsequent cellulose activation *via* glycosidic bond cleavage.

Another common characteristic of the preactivated $B_{O,3}$ and $^{1}C_{4}$ conformations is that the C1-O1 bond is poised in the axial orientation, enabling a new intramolecular hydrogen bond between the O6 hydroxymethyl group and glycosidic oxygen atom O1. Figure 2c shows the distances of O6-H6···O1 of each lowest-energy methyl-cellobiose conformation considered. To illustrate the distance below which is considered a hydrogen bond, the region below 3.2 Å is shaded with light blue. The $B_{O,3}$ conformation has the shortest O6-H6···O1 distance of 1.97 Å, indicating a moderate intramolecular hydrogen bond. The $^{1}C_{4}$ conformation has the second shortest O6-H6···O1 distance of 2.46 Å, indicating a weak intramolecular hydrogen bond. On the other hand, the O6-H6···O1 distances are greater than 3.2 Å for all three inactivated conformations ($^{4}C_{1}$, $^{3}S_{1}$, and $B_{1,4}$), in which the equatorial C1-O1 alignment impedes the O6 hydroxymethyl group to carry out nucleophilic attack on the anomeric carbon atom C1 for glycosidic bond activation.

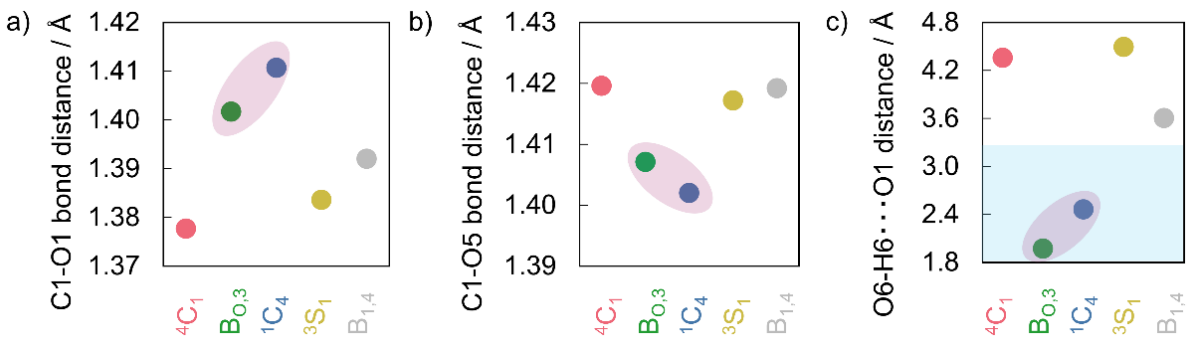

Figure 2. The distances of **a)** C1-O1 bond, **b)** C1-O5 bond, and **c)** O6-H6···O1 of the five lowest-energy methyl-cellobiose conformations. Purple shaded region highlights the values for the conformations that are structurally favorable to undergo subsequent concerted glycosidic bond cleavage. The hydrogen bond region in **c)** is shaded in light blue.

3.3. Cellulose Activation *via* Glycosidic Bond Cleavage

3.3.1. Methyl-Cellobiose Activation

Starting from the two preactivated conformations ($B_{O,3}$ and $^{1}C_{4}$), two possible itineraries were identified by our IRC calculations for cellulose activation *via* concerted glycosidic bond cleavage: $B_{O,3} \rightarrow {}^{2}S_{O}^{\ddagger} \rightarrow$ Products and $^{1}C_{4} \rightarrow {}^{5}H_{4}^{\ddagger} \rightarrow$ Products.

For both itineraries, two mechanisms of concerted glycosidic bond cleavage are examined. The first mechanism, designated as Mechanism I, considers proton transfer from the hydroxymethyl group and intramolecular nucleophilic attack by the same hydroxymethyl group at the same time, as described by Mayes et al.[14] The second mechanism, designated as Mechanism II, is a new concerted mechanism proposed in this work that considers the effects caused by the intramolecular hydrogen bonds between the adjacent hydroxyl and hydroxymethyl groups in addition to the elementary events in Mechanism I. Detailed discussions of both mechanisms for both itineraries are provided in this section.

3.3.1.1. Concerted Mechanism I

Figure 3 shows the TSs *via* Mechanism I following the two itineraries and the corresponding local minima identified by the IRC calculations. In Mechanism I, the proton H6 from the O6 hydroxymethyl group is transferred to the glycosidic oxygen atom O1 while the oxygen atom O6 involves in a nucleophilic attack to the electrophile carbon atom C1, leading to the formation of the C1-O6 bond between the nucleophile and the carbocation and a bicyclic ring. **TS1** in ${}^{2}S_{O}^{\ddagger}$ is the same transition state structure reported by Mayes et al.[14] The reactant **S4** leading to **TS1** is poised in the $B_{O,3}$ conformation (Figure 3a). **TS2** in ${}^{5}H_{4}^{\ddagger}$ is identified as the transition state linked to the reactant **S5** in the $^{1}C_{4}$ conformation (Figure 3b). Both TSs and their corresponding reactants have the hydroxymethyl group of the non-reducing end in the GG orientation.

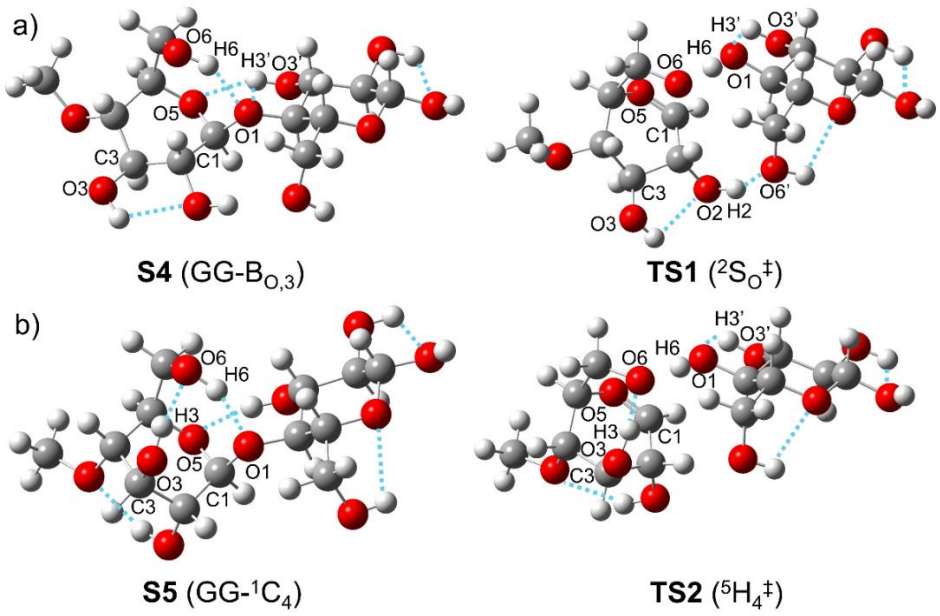

254

255 **Figure 3.** TSs of methyl-cellobiose activation *via* Mechanism I in the syn conformation. **a) TS1** in $^{2}S_{O}^{‡}$ and
256 its corresponding local minimum **S4** in $B_{O,3}$ and **b) TS2** in $^{5}H_{4}^{‡}$ and its corresponding local minimum **S5** in
257 $^{1}C_{4}$. Blue dotted lines represent hydrogen bonds.

258 The rate parameters of methyl-cellobiose activation *via* Mechanism I are listed in Table 1. The syn-$^{1}C_{4}$
259 itinerary through **TS2** has an energy barrier of 51.3 kcal mol^{-1}, 4.1 kcal mol^{-1} lower than the syn-$B_{O,3}$
260 itinerary through **TS1**. To discern the main difference between the two preactivated $B_{O,3}$ and $^{1}C_{4}$
261 conformations, the O3-H3···O6 distance is examined as a possibility of forming another intramolecular
262 hydrogen bond. The equatorial C3-O3 alignment in $B_{O,3}$ (Figure 3a) prohibits an intramolecular hydrogen
263 bond between the O3 hydroxyl and O6 hydroxymethyl groups, while a moderate intramolecular O3-H3···
264 O6 hydrogen bond with a length of 1.8 Å is observed in the $^{1}C_{4}$ conformation (Figure 3b) because of the
265 C3-O3 bond poised in the axial orientation. This intramolecular O3-H3···O6 hydrogen bond present in the
266 $^{1}C_{4}$ conformation makes the O6 hydroxymethyl group more susceptible for initiating a nucleophilic attack
267 on C1, the main reason responsible for the lower activation energy of the syn-$^{1}C_{4}$ itinerary.

268 Although the low activation energy of the syn-$^{1}C_{4}$ itinerary for cellulose activation during pyrolysis has not
269 been reported in the literature, DFT studies on other carbohydrate compounds have shown similar behaviors.

Seshadri et al.[31] reported that in β-D-glucose pyrolysis, the $^1C_4$ itinerary is approximately 7 kcal mol^{-1} more energetically favorable than the $B_{O,3}$ itinerary. Hosoya et al.[15] reported that the activation energy of cellobiose pyrolysis from the $^1C_4$ itinerary is approximately 13 kcal mol^{-1} lower than that from the syn-$B_{O,3}$ itinerary, although the $^1C_4$ structure studied in their work is in the anti conformation. Since native cellulose is experimentally observed in the syn conformation,[59, 60] and cellulose has a highly packed structure consisting of stacked parallel sheets, the syn-to-anti isomerization of β-D-glucopyranose rings is unfavorable.[14, 35] The syn-$^1C_4$ itinerary discovered in our work thus represents a more realistic mechanism as opposed to the anti-$^1C_4$ itinerary. Detailed discussions of methyl-cellobiose pyrolysis in the anti conformation can be found in Section S3 of SI.

Table 1. Arrhenius parameters and rate constant for concerted glycosidic bond cleavage of methyl-cellobiose at the M06-2X/6-31+G(2df,p) level of theory.

Index	Itinerary	Mechanism type	A (s^{-1})	E_a (kcal mol^{-1})	k at 773.15 K (s^{-1})
TS1	syn-$B_{O,3}$	I	5.4 x 10^{12}	55.4	1.2 x 10^{-3}
TS2	syn-$^1C_4$	I	2.0 x 10^{12}	51.3	6.2 x 10^{-3}
TS3	syn-$B_{O,3}$	II	7.2 x 10^{12}	56.0	1.0 x 10^{-3}
TS4	syn-$^1C_4$	II	2.1 x 10^{12}	47.4	8.0 x 10^{-2}

It is important to compare the structures of methyl-levoglucosan (MLG), the product of methyl-cellobiose activation that represents "active cellulose". In this work, two distinct MLG conformations were found, one for each itinerary. MLG from the $B_{O,3}$ itinerary has the $B_{O,3}$ conformation with two hydrogen bonds between the equatorial hydroxyl groups, while MLG from the $^1C_4$ itinerary is poised in the $^1C_4$ conformation with three hydrogen bonds between the axial hydroxyl groups. Thus, the most stable MLG structure at 773.15 K has the $^1C_4$ conformation, where the Gibbs free energy of MLG in the $B_{O,3}$ conformation is 2.1 kcal mol^{-1} higher than that of the most stable structure in $^1C_4$. This finding is supported by the theoretical[65] and neutron diffraction[66] studies, where the most stable structure of LG adapts the $^1C_4$ conformation. Section S4 of SI

contains a list of low-energy structures of the products from methyl-cellobiose activation *via* glycosidic bond cleavage.

3.3.1.2. Concerted Mechanism II

The potential energy surface was searched for cellulose activation *via* Mechanism II for both $B_{O,3}$ and $^{1}C_{4}$ itineraries. Figure 4 demonstrates the TSs of the syn-$B_{O,3}$ and the syn-$^{1}C_{4}$ itineraries *via* Mechanism II and the corresponding local minima identified by the IRC calculations. **TS3** in $^{2}S_{O}^{‡}$ corresponds to **S6** in $B_{O,3}$ (Figure 4a), and **TS4** in $^{5}H_{4}^{‡}$ corresponds to **S7** in $^{1}C_{4}$ (Figure 4b). Both TSs and corresponding local minima have the hydroxymethyl group of the non-reducing end unit in the GG orientation.

Mechanism II involves the same events of Mechanism I with additional breaking and formation of intramolecular hydrogen bonds between the O6 hydroxymethyl group and the O3' hydroxyl group. As illustrated in Figure 4, the O6 hydroxymethyl group of the non-reducing end of both **S6** in $B_{O,3}$ and **S7** in $^{1}C_{4}$ donates a hydrogen bond (red dotted lines in Figure 4) to the O3' hydroxyl group of the reducing end, leading to a local bifurcated hydrogen bond. In the TSs, this local bifurcated hydrogen bond is broken, and the O3' hydroxyl group is allowed to subsequently rotates and donates a hydrogen bond to the O6 hydroxymethyl group (green dotted lines in Figure 4), while the hydrogen atom H6 from O6 is simultaneously transferred to O1. In contrast with **S6** and **S7**, the O3' hydroxyl group of **S4** and **S5** donates a hydrogen bond to the ring oxygen atom O5 in Mechanism I (Figure 3), impeding the formation of a hydrogen bond with the O6 hydroxymethyl group.

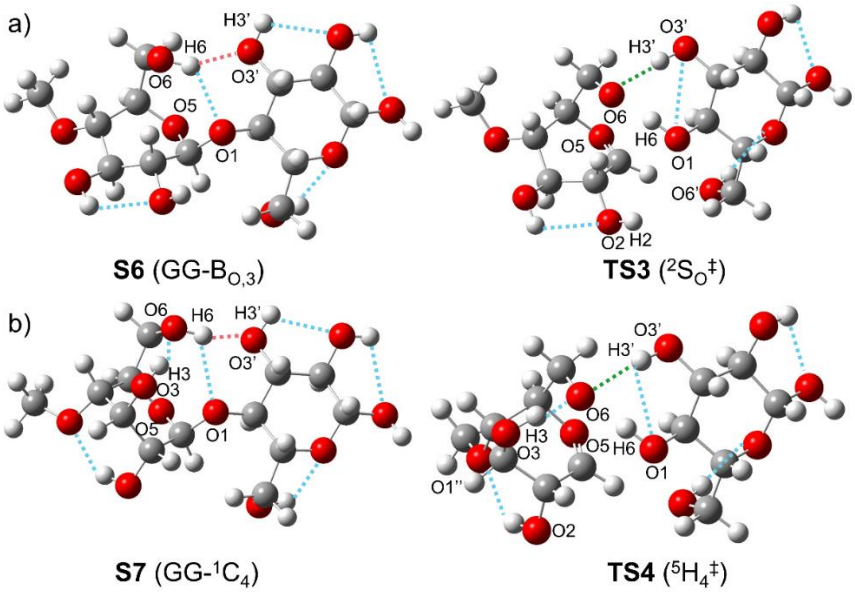

307

308 **Figure 4.** TSs of methyl-cellobiose activation *via* Mechanism II in the syn conformation. **a) TS3** in $^2S_O^‡$ and
309 its corresponding local minimum **S6** in $B_{O,3}$ and **b) TS4** in $^5H_4^‡$ and its corresponding local minimum **S7** in
310 $^1C_4$. Blue, red, and green dotted lines represent intact, broken, and new hydrogen bonds, respectively.

311 The rate parameters of methyl-cellobiose activation *via* Mechanism II are compared to those *via* Mechanism
312 I in Table 1. The O3' hydroxyl group near the reaction center stabilizes the O6 hydroxymethyl group in the
313 TSs (**TS3** and **TS4** in Figure 4). Notable difference in the energetics due to this stabilizing effect caused by
314 the presence of intramolecular O3'-H3'···O6 hydrogen bond was observed for the syn-$^1C_4$ itinerary,
315 leading to a 3.9 kcal mol^{-1} reduction in the activation energy for **TS4** *via* Mechanism II compared to **TS2**
316 *via* Mechanism I. Overall, an order of magnitude increase in the rate constant for the syn-$^1C_4$ itinerary was
317 estimated at this reaction temperature (773.15 K).

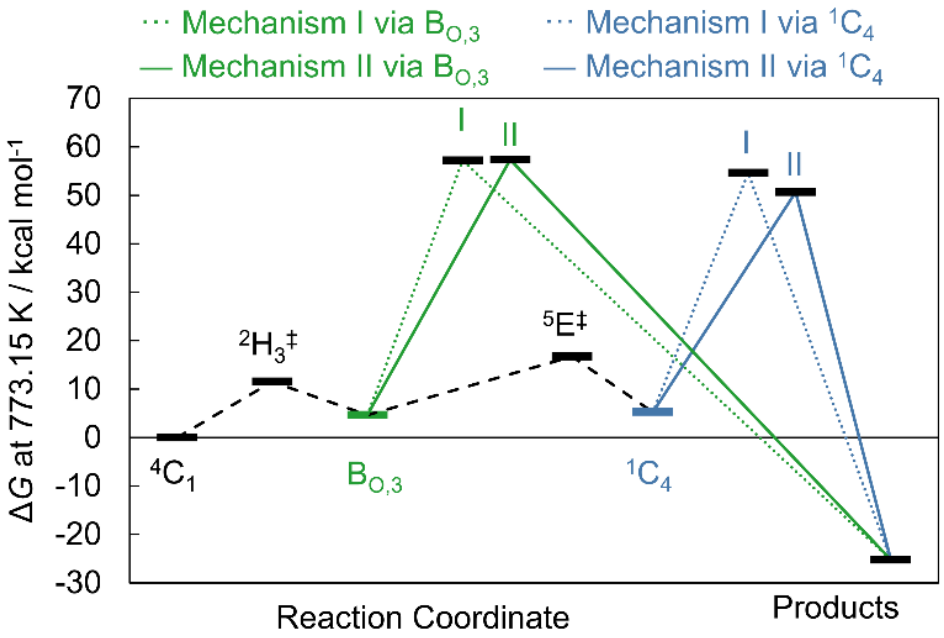

318

319 **Figure 5.** Gibbs free energy surface of methyl-cellobiose pseudorotational ring puckering (black dash lines)
320 from the most stable $^4C_1$ conformation to the preactivated conformations and activation from the syn-$B_{O,3}$
321 and syn-$^1C_4$ itineraries, calculated at the M06-2X/6-31+G(2df,p) level of theory. Black double daggers
322 correspond to the TSs of ring puckering interconversions. Methyl-cellobiose activation *via* Mechanism I
323 (dotted line) and Mechanism II (solid line) discussed in this work are both illustrated. $^2H_3‡$ and $^5E‡$ are the
324 conformations of the TSs for $^4C_1 \rightarrow B_{O,3}$ and $B_{O,3} \rightarrow {}^1C_4$ isomerization, respectively. The combined Gibbs
325 free energy values of MLG and glucose is used to represent the total Gibbs free energy level of the products.

326 The Gibbs free energy surface along the reaction coordinate of methyl-cellobiose isomerization and
327 activation is summarized in Figure 5. For cellulose activation, the syn-$^1C_4$ itinerary *via* Mechanism II (blue
328 solid line) is the most favorable route. The calculated activation barrier for intermediate isomerization (i.e.,
329 pre-activation) steps from $^4C_1$ to $^1C_4$ in the methyl-cellobiose model was found to be significantly lower
330 than that for methyl-cellobiose activation *via* concerted glycosidic bond cleavage (by 33 kcal mol^{-1}). Even
331 considering the possible local environmental effects induced by interchain hydrogen bonds, which could
332 reduce its activation energy by 1–12 kcal mol^{-1}, the glycosidic bond cleavage reaction is still the rate-limiting
333 step during cellulose fast pyrolysis compared to pre-activation ring puckering.

Our calculations reveal that cellulose undergoes pseudorotation during its pyrolysis to reach a favorable conformation (i.e., syn-$^{1}C_{4}$) before activation. In Mechanism II, the transition state of concerted glycosidic bond cleavage is stabilized by intramolecular hydrogen bonds connected to the adjacent O3' hydroxyl group, lowering its reaction barrier and allowing it to become the more favorable cellulose activation pathway.

Stabilization by external hydrogen bonds to accelerate carbohydrate pyrolysis have been reported in the literature. For example, Seshadri et al.[31] suggest that explicit hydroxylated molecules, such as water, facilitate the concerted mechanism of β-D-glucose pyrolysis, lowering the reaction barrier by 6.6 kcal mol^{-1}. Maliekkal et al.[29] suggest that transglycosylation of cellulose could be catalyzed by hydroxyl groups of a neighboring sheet at low temperatures (< 467 °C), where this inter-sheet hydroxyl-catalyzed pathway leads to a low activation barrier of 29.5 kcal mol^{-1} as opposed to 51–59 kcal mol^{-1} at temperatures > 467 °C. Similar effect caused by intramolecular hydrogen bond in the vicinity of the reaction center, however, has never been explored. The methyl-cellobiose activation *via* Mechanism II discovered in this work shows for the first time that the stabilization of the transition state by an intramolecular hydrogen bond with the adjacent pyranose ring within the same cellulose chain is possible during cellulose activation *via* glycosidic bond cleavage. Note that the hydroxyl-activated mechanism discussed in our work, driven by *intramolecular* hydrogen bonds, is envisioned as non-catalytic and drastically different from the catalytic acceleration mechanism discussed in Maliekkal et al.,[29] where a neighboring cellulose sheet is required as an external hydrogen donor to catalyze the reaction. Consequently, the Maliekkal et al. mechanism is expected to be dominant at temperatures lower than 467 °C, where cellulose sheets are more intact before phase transition and a neighboring cellulose sheet is more accessible. On the other hand, our mechanism focuses on intrachain effects at high temperatures (> 467 °C) and therefore steric hindrance caused by a neighboring cellulose sheet is expected to play a lesser role.

3.3.2. One-Chain Activation

To further examine the effects of model size on the accuracy of activation energy predictions, cellulose activation was studied using a one-chain model. Cellotetraose containing a reducing end, a non-reducing

end, and two interior units was employed to mimic a single cellulose chain. A thorough analysis of selecting this one-chain structure is presented in Section S5 of SI. A 2-layer ONIOM method with the M06-2X/6-31+G(2df,p):M06-2X/6-31G(d,p) level of theory was employed in this section. A rigorous discussion of the validity of selecting the 2-layer ONIOM method used in this study is given in Section S6 of SI. The CHelpG partial charges were calculated at the M06-2X/6-31+G(2df,p) level of theory. Section S7 of SI contains the structural and energetic information of the low-energy stable conformers and TSs examined by the one-chain model.

Since the glycosidic bond cleavage reaction is expected to be the rate-limiting step during cellulose fast pyrolysis, having activation energy 21–32 kcal mol^{-1} higher than pre-activation ring puckering, we did not attempt to study pre-activation ring puckering from $^4C_1$ to $^1C_4$ via the larger one-chain and two-chain models, whose main objective was to quantitatively obtain more accurate kinetic parameters rather than to identify molecular-level reaction pathways (which was achieved by the smaller methyl-cellobiose model).

To identify the lowest-energy conformer of the one-chain model, cellotetraose structures starting with three different orientations of the hydroxymethyl groups (TG, GG, and GT) were explored. Different hydrogen bonding patterns were also considered by performing the dihedral scans around the hydroxymethyl torsion angles. Figure 6a shows the lowest-energy structure (**C1-S1**) of the one-chain model in the TG orientation.

Native cellulose is experimentally known to have two hydrogen bond networks, namely Network A and Network B, based on the alternative hydrogen positions of the O2 and O6 functional groups.[59, 60] Both networks have the intramolecular hydrogen bond between the O3 hydroxyl group and O5 ring oxygen atom (e.g., O3'-H3'···O5, the purple dotted line in Figure 6a). In Network A, the O6 hydroxymethyl group accepts a hydrogen bond from the O2 hydroxyl group (e.g., O2'-H2'···O6''', the orange dotted line in Figure 6c), whereas, in Network B, the O6 hydroxymethyl groups donates a hydrogen bond to the O2 hydroxyl groups (e.g., O6'-H6'···O2, the green dotted line in Figure 6a).

382 The scission of cellotetraose can take place at three possible sites: between the non-reducing end and its
383 neighboring interior unit, designated as Sc1; between two interior units, designated as Sc2; and between the
384 reducing end and its neighboring interior unit, designated as Sc3. In the one-chain model, cellulose
385 activation was investigated following the syn-$^{1}C_{4}$ itinerary *via* Mechanism II, the most favorable route
386 discovered for methyl-cellobiose activation. Initial transition state guesses were constructed by replacing
387 any two neighboring β-D-glucopyranose units in the one-chain model with the structure of **TS4** (Figure 4).
388 Figure 6b-d shows the lowest-energy TSs at three different scission sites. All TSs have the most stable $^{4}C_{1}$
389 conformation except the unit carrying out the nucleophilic attack, which has the $^{5}H_{4}^{\ddagger}$ conformation in the
390 GG orientation, the same as the corresponding unit of **TS4** for methyl-cellobiose activation.

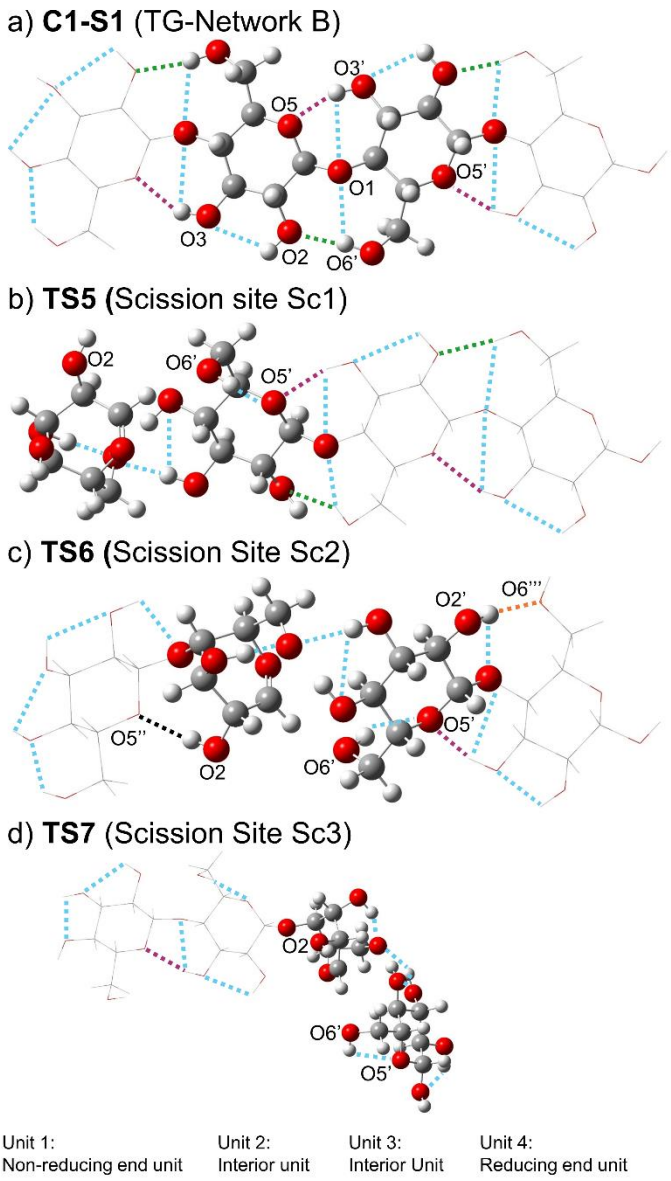

391

392 **Figure 6. a)** The lowest-energy one-chain structure (**C1-S1**) in the TG-Network B orientation and the syn
393 conformation. Each unit is poised in $^4C_1$. TSs represent cellulose activation *via* Mechanism II at the scission
394 sites of **b)** Sc1 (**TS5**), **c)** Sc2 (**TS6**), and **d)** Sc3 (**TS7**) in the syn conformation. Units are numbered starting
395 from the non-reducing end. Dotted lines represent hydrogen bonds.

396 The rate parameters for the one-chain activation reaction *via* Mechanism II at three scission sites are
397 summarized in Table 2. The activation energies were determined to be between 49.3 kcal mol^{-1} and 53.5
398 kcal mol^{-1}. To understand the effects of the different scission sites, the intramolecular hydrogen bonding of

399 the three TSs were further examined. As illustrated in Figure 6b-d, the high activation energy of **TS7** can
400 be attributed to three fewer hydrogen bonds and more distorted structure compared to **TS5** and **TS6**. Even
401 though **TS5** and **TS6** have the same number of intramolecular hydrogen bonds, cellotetraose activation at
402 Sc2 (**TS6**) is 3.3 kcal mol^{-1} more favorable than Sc1 (**TS5**). The main difference is that the O2 hydroxyl
403 group donates a hydrogen bond solely in Sc2, where the intramolecular O2-H2···O5'' hydrogen bond
404 stabilizes the transition state (the black dotted line in Figure 6c), resulting in the lowest-energy barrier at
405 49.3 kcal mol^{-1}. These calculation results suggest that cellulose activation is more favorable to take place
406 between the interior units.

407 **Table 2.** Arrhenius parameters and rate constant for cellotetraose activation *via* Mechanism II glycosidic
408 bond cleavage at ONIOM(M06-2X/6-31+G(2df,p):M06-2X/6-31G(d,p)) level of theory.

Index	Chain scission site	Conformation	A (s^{-1})	E_a (kcal mol^{-1})	k at 773.15 K (s^{-1})
TS5	Sc1	TG – Network B	9.1×10^{12}	52.6	1.2×10^{-2}
TS6	Sc2	TG – Network A	8.7×10^{12}	49.3	9.8×10^{-2}
TS7	Sc3	GG	3.5×10^{13}	53.5	2.7×10^{-2}

409 Interestingly, the conformational changes are not limited to the reaction center, but also observed in adjacent
410 units of the reaction center. The hydroxymethyl group of the reducing end in **TS6** rotates to accept a
411 hydrogen bond from the O2' group of Unit 3 (O2'-H2'···O6''', the orange dotted line in Figure 6c), while
412 the hydroxymethyl groups of Units 1 and 2 in **TS7** rotates out-of-plane to reside in the GG orientation,
413 preventing hydrogen bonds from connecting to these hydroxymethyl groups (Figure 6d). On the other hand,
414 the hydroxymethyl groups of Units 3 and 4 in **TS5** (Figure 6b) remain in the TG orientation, allowing the
415 same intramolecular hydrogen bonding (Network B), as seen in the lowest-energy structure (**C1-S1** in Figure
416 6a).

417 To distinguish the effects of adjacent units on cellulose activation, the structures of the TSs from the methyl-
418 cellobiose and cellotetraose models were further compared. In the absence of a neighboring unit in the

methyl-cellobiose model (**TS4** in Figure 4b), the O2 group donates a hydrogen bond to the O1'' glycosidic oxygen atom, while the reducing end unit in **TS6** inhibits this hydrogen bond and allows the intramolecular O2-H2···O5'' hydrogen bond (the black dotted line in Figure 6c). This steric hindrance caused by the adjacent unit in the one-chain model results in an increase of 1.9 kcal mol^{-1} in the activation energy compared to the methyl-cellobiose model.

3.3.3. Two-Chain Activation

Our QC calculations in this section focus on the effects of interchain hydrogen bonds between two cellulose chains in the same sheet during cellulose pyrolysis. A two-chain model consisting of two cellotetraose directed in the same orientation was employed. In this model, the top chain is considered as the reactive chain, where glycosidic bond cleavage occurs. The bottom chain serves as the assisting chain, where no reaction takes place. Section S8 of SI contains the structural and energetic information of low-energy stable conformers and TSs considered in the two-chain model. All calculations were performed using the 2-layer ONIOM approach at the ONIOM(M06-2X-D3/6-31+G(2df,p):M06-2X-D3/6-31G(d,p)) level of theory in this section. The CHelpG partial charges were calculated at the M06-2X/6-31+G(2df,p) level of theory. The comparison of dispersion-corrected and uncorrected results can be found in Section S9 of SI.

Figure 7a shows the lowest-energy structure (**C2-S1**) in the TG orientation in Network A. Cellulose activation in the two-chain model was investigated between the interior units of the top chain following the syn-$^{1}C_{4}$ itinerary *via* Mechanism II discovered in the methyl-cellobiose model. An initial guess was constructed by replacing the two interior units of the top chain of **C2-S1** with the structure of **TS4** (Figure 4b). Figure 7b demonstrates **TS8** for cellulose activation in the two-chain model. All units of **TS8** have the $^{4}C_{1}$ conformation except the unit carrying out the nucleophilic attack (i.e., Unit 2 of the top chain in Figure 7b), which has the $^{5}H_{4}^{\ddagger}$ conformation in the GG orientation.

Using this two-chain model, the pre-exponential factor and the rate constant at 773.15 K were determined to be 4.3 x 10^{12} s^{-1} and 1.9 x 10^{-2} s^{-1}, respectively. The activation energy was calculated as 50.8 kcal mol^{-1}.

The cellulose activation in the two-chain model follows the same mechanism in the one-chain and methyl-cellobiose models. Both two-chain and one-chain models include the intramolecular O2-H2···O5'' hydrogen bond (the black dotted line in Figure 7b), which stabilizes the transition state. Compared to the one-chain model, introducing the interchain hydrogen bonds in the two-chain model leads to an increase in the activation energy of cellulose activation by approximately 1.5 kcal mol^{-1}. This suggests that the assisting (bottom) chain acts an inhibitor in cellulose activation.

To explain the effects of the assisting (bottom) chain on cellulose activation, the interchain hydrogen bonds were further examined. In the absence of the interchain hydrogen bonds in the methyl-cellobiose and one-chain models, the O6' hydroxymethyl group has the freedom to rotate out-of-plane and resides in the GG orientation in the transition states (reducing end of **TS4** in Figure 4b and Unit 3 of **TS6** in Figure 6c). Our calculations show that in the two-chain model, the rotation of the hydroxymethyl group of Unit 3 of the top chain is impeded due to the presence of an interchain O6'-H6'···O3b' hydrogen bond (the purple dotted line in Figure 7b). The stabilization provided by the intramolecular O6'-H6'···O5' hydrogen bond in the one-chain model (Figure 6c) is not present in the two-chain model. This finding is consistent with the simulations performed by Agarwal et al., [67] which suggests that intrachain hydrogen bonds at the O6 location are converted into weaker interchain hydrogen bonds between 400 and 450 K during phase transition. The steric hindrance caused by the O6'-H6'···O3b' interchain hydrogen bond destabilizes the transition state of the two-chain model, increasing the activation energy for the mid-chain cellulose activation reaction by 1.5 kcal mol^{-1}, from 49.3 kcal mol^{-1} to 50.8 kcal mol^{-1}. This increase, however, is small compared to the magnitude of the activation energy and thus the steric hindrance due to phase transition is not expected to play a significant role for the mid-chain cellulose activation reaction considered in this work.

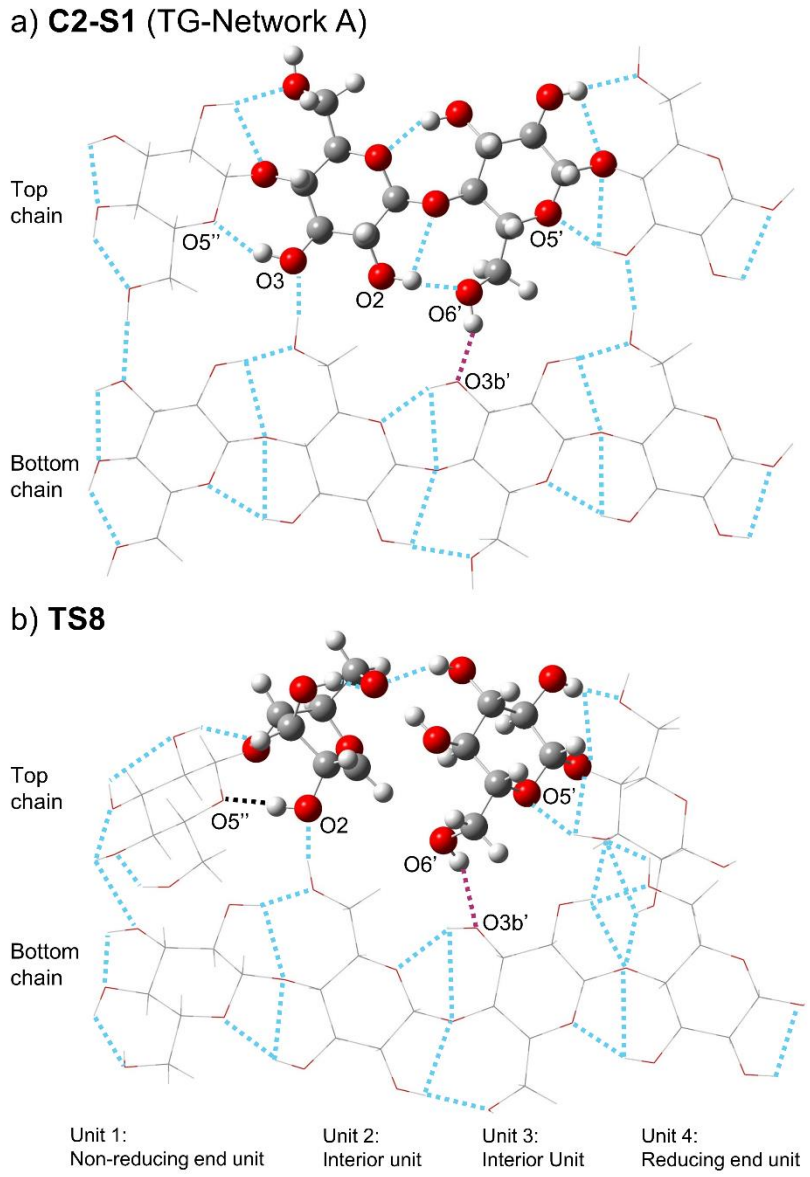

464

465 **Figure 7.** The lowest-energy structures of **a)** the two-chain cellotetraose (**C2-S1**) and **b)** the transition state

466 (**TS8**) for cellulose activation *via* Mechanism II in the syn conformation. Units are numbered starting from

467 the non-reducing end. Dotted lines represent hydrogen bonds.

3.4. LG Formation from Active Cellulose

3.4.1. LG Formation Studied by Methyl-Cellobiosan

Once a cellulose chain is activated *via* glycosidic bond cleavage, the "active cellulose" can subsequently undergo successive glycosidic bond cleavage to form LG molecules. To study the mechanism of LG formation, methyl-cellobiosan, which is cellobiosan with a methyl group added to its non-reducing end, was used as a model "active cellulose" compound in our calculations. Methyl-cellobiosan with the LG-end in both $B_{O,3}$ and $^{1}C_{4}$ conformations was studied. The possible rotation of the LG end from the syn to anti conformations was also considered when searching for the lowest-energy methyl-cellobiosan conformer. The dihedral angle scan on the potential energy surface reveal that the LG end of methyl-cellobiosan is most stable in the syn-$^{1}C_{4}$ conformation, shown as **S8** in Figure 8a. The non-reducing end of methyl-cellobiosan was found to be in the $^{4}C_{1}$ conformation and the GG orientation. Structures and relative energies of several other low-energy methyl-cellobiosan conformers are included in Section S10 of SI.

Figure 8b shows the transition state of LG formation from methyl-cellobiosan decomposition *via* concerted glycosidic bond cleavage, along with the corresponding reactant (**S9**) identified by the IRC calculations. Our calculations show that the reaction follows the same itinerary defined by $^{1}C_{4} \rightarrow {}^{5}H_{4}^{\ddagger} \rightarrow$ Products as methyl-cellobiose activation. **S9** is poised in the $^{1}C_{4}$ conformation with the hydroxymethyl group of the non-reducing end in the GG orientation. Section S11 of SI contains several low-energy structures of LG.

Our findings also suggest that concerted glycosidic bond cleavage of methyl-cellobiosan follows the same elementary events of Mechanism I. The pre-exponential factor and the rate constant at 773.15 K were determined to be 2.3×10^{12} s^{-1} and 1.5×10^{-2} s^{-1} using the transition state theory, respectively. The activation energy was calculated to be 50.2 kcal mol^{-1}.

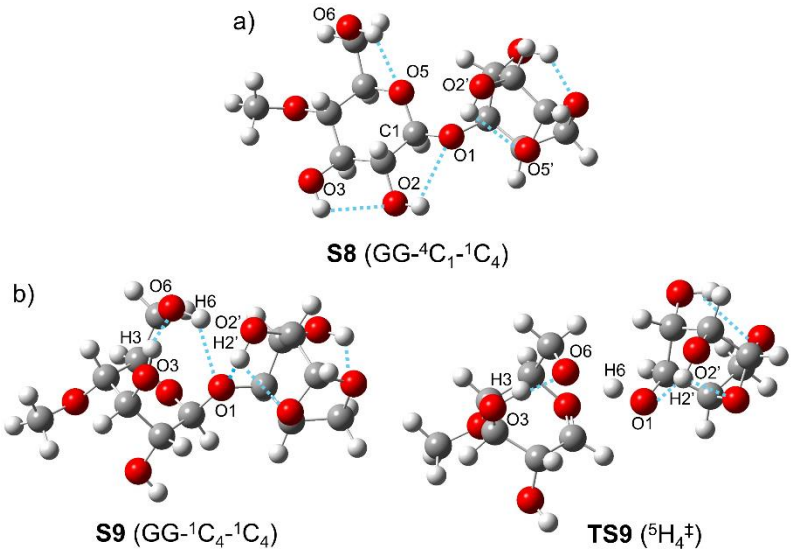

Figure 8. a) The lowest-energy structure of methyl-cellobiosan in the syn conformation (**S8**). The non-reducing and the LG ends are poised in the $^{4}C_{1}$ and $^{1}C_{4}$ conformations, respectively. **b)** Structures of the transition state (**TS9**) in $^{5}H_{4}^{‡}$ and its corresponding local minimum (**S9**) in $^{1}C_{4}$ for LG formation from methyl-cellobiosan decomposition *via* concerted glycosidic bond cleavage in the syn conformation. Blue dotted lines represent hydrogen bonds.

3.4.2. LG Formation Studied by One-Chain Model

The depolymerization of "active cellulose" was investigated using cellotetrasan, which resembles cellotetraose but with the reducing end replaced with an LG end. For the search of the lowest-energy structure of cellotetrasan, the initial guesses were constructed using the lowest-energy cellotetraose conformations, with the reducing end replaced with the LG-end unit of **S8** (Figure 8a). The potential energy surface was explored starting from various hydrogen bond networks following the same conformational search procedure of cellotetraose. Figure 9a shows the lowest-energy cellotetrasan (**C1-S2**), where all units have the TG-$^{4}C_{1}$ conformation in Network B, except the LG-end unit, which has the $^{1}C_{4}$ conformation.

The search of the TS started with replacing the Units 3 and 4 of **C1-S2** with the structure of **TS9** (Figure 8b). Figure 9b displays **TS10** for the LG formation in the one-chain model. The pre-exponential factor and

rate constant at 773.15 K were determined to be 7.7 x 10^{12} s^{-1} and 6.9 x 10^{-3} s^{-1} using the transition state theory, respectively. The activation energy was calculated as 53.2 kcal mol^{-1}.

Glycosidic bond cleavage is not affected by the steric effects in LG formation in contrast to cellulose activation. Since the end unit has more freedom to rotate compared to the interior units, the reactive units of **TS10** (Units 3 and 4 in Figure 9b) are more distorted compared to those of **TS6** (Units 2 and 3 in Figure 6c), enabling an intramolecular O2-H2···O1'' hydrogen bond. Increasing the chain length from two to four units results in an increase in the activation energy by 3.0 kcal mol^{-1}, even though the concerted mechanism for LG formation in the one-chain model is the same as that in the methyl-cellobiosan model. The adjacent units in the one-chain model perturb the electronic structure of the reactive units, where a notable difference in the CHelpG partial charge on the O5 ring oxygen atom of the reactive units was observed. Comparing non-reducing end of **S8** (Figure 8a) and Unit 3 of **C1-S2** (Figure 9a) shows that 0.36 au more negative charge is distributed to the O5 atom (partial charge of −0.71 au) in the presence of the adjacent units. As a result, **S8** is more susceptible to nucleophilic attack than **C1-S2**. It is also evident that **S8** is more favorable to nucleophilic attack because of its elongated C1-O1 bond and the shortened C1-O5 bond compared to **C1-S2**.

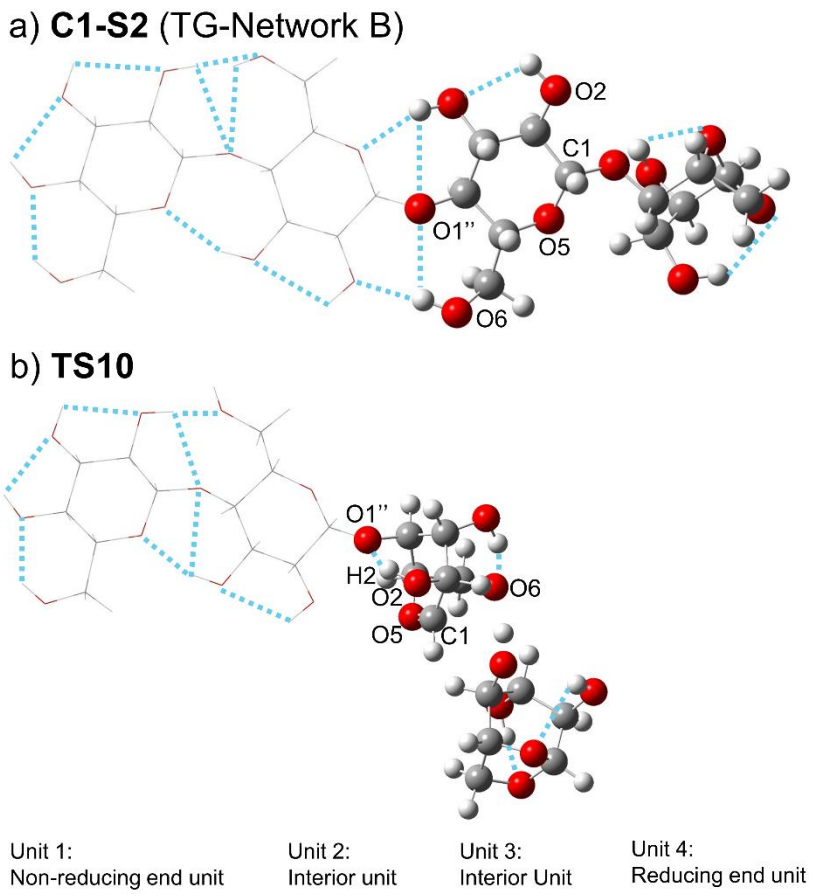

Figure 9. The lowest-energy structures of **a)** cellotetrasan (**C1-S2**) and **b)** transition state (**TS10**) used in the one-chain model for studying LG formation from concerted glycosidic bond cleavage of active cellulose in the syn conformation. Units are numbered starting from the non-reducing end. Blue dotted lines represent hydrogen bonds.

3.4.3. LG Formation Studied by Two-Chain Model

The formation of LG was further studied using the two-chain model with cellotetrasan as the top (reactive) chain and cellotetraose as the bottom (assisting) chain. The top chain represents anhydrosugar intermediate with LG end chain, which undergoes successive glycosidic bond cleavage in the depolymerization step.

C2-S1 (Figure 7a) was used to construct the initial guesses, where the reducing end unit of the top chain was replaced with the LG-end of **S8** (Figure 8a). Figure 10a displays the lowest-energy structure (**C2-S2**)

of the two-chain model representing "active cellulose". All units have the $^4C_1$ conformation in the TG orientation except the LG-end of the top chain, which has the $^1C_4$ conformation.

The initial guesses for the TS were built by replacing the interior Unit 3 and the LG-end Unit 4 of the top chain of **C2-S2** with the structure of **TS9** (Figure 8b). Figure 10b shows **TS11** of the two-chain active cellulose model for LG formation. The activation energies calculated from the two-chain model indicates that cellulose activation (E_a = 50.8 kcal mol^{-1}) is energetically more challenging than the subsequent LG formation *via* cellulose depolymerization (E_a = 40.9 kcal mol^{-1}). The pre-exponential factor and the rate constant at 773.15 K were determined to be 1.9 x 10^{12} s^{-1} and 5.2 s^{-1}, respectively. Furthermore, the activation energy of LG formation in the two-chain model decreased by 12.3 kcal mol^{-1} compared to that in the one-chain model. As a result, the assisting (bottom) chain serves as a catalyst for LG formation, as opposed to an inhibitor in cellulose activation.

Further examination of **TS11** (Units 3 and 4 of the top chain in Figure 10b) illustrates how the top and bottom chains are rigidly held in a conformation that does not allow the end unit to have the freedom to rotate out-of-plane as opposed to **TS10** (Units 3 and 4 in Figure 9b). Structural tightening occurs in the transition state *via* two additional hydrogen bonds in the two-chain model. First, the LG-end (Unit 4) of the top chain is bound to the bottom chain *via* the interchain O6b'-H6b'···O3' hydrogen bond (the purple dotted line in Figure 10b). Second, Unit 3 is connected *via* the intramolecular O2-H2···O5'' hydrogen bond (the black dotted line in Figure 10b) in the top chain due to the restriction of the out-of-plane motion caused by the interchain hydrogen bonds. It is evident from the comparison to **TS6** (Figure 6c) that this O2-H2···O5'' hydrogen bond stabilizes the transition state, and thus lowers the activation energy.

Noncovalent interactions between the top and bottom chains perturb the atomic and electronic structures of the TSs in favor of glycosidic bond cleavage. Comparing the unit carrying out the nucleophilic attack of the TSs between **TS11** (Unit 3 of the top chain in Figure 10b) and **TS10** (Unit 3 in Figure 9b) shows a 0.19 au more negative charge distributed to the O6 atom (partial charge of −0.89 au) in the presence of the assisting

555 (bottom) chain. This shortened C1-O5 bond of **TS11** allows for more positive partial charge by 0.18 au on
556 the C1 atom (partial charge of 0.40 au) as opposed to **TS10**. Our calculation results suggest that noncovalent
557 interactions caused by the assisting chain makes the reactive (top) chain more susceptible to nucleophilic
558 attack for LG formation.

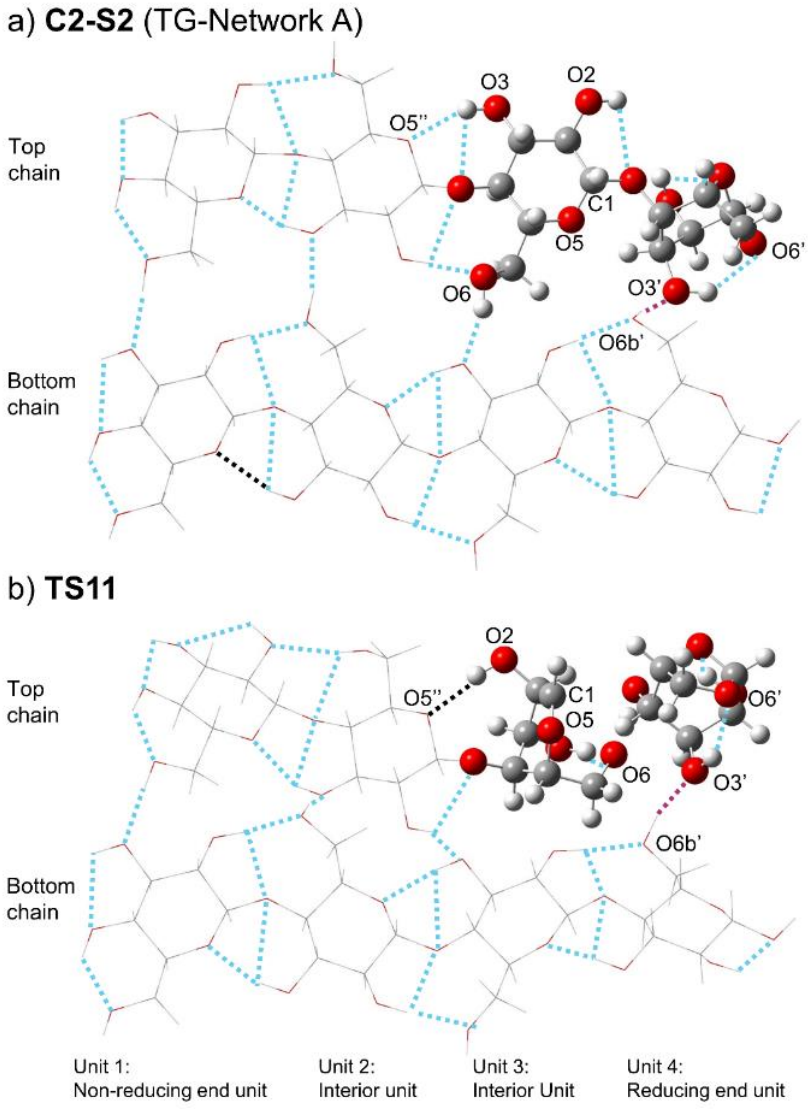

559

560 **Figure 10.** The lowest-energy structure of **a)** LG-end reactant (**C2-S2**) and **b)** the transition state (**TS11**) of
561 the two-chain model representing cellulose depolymerization in the syn conformation. Units are numbered
562 starting from the non-reducing end. Dotted lines represent hydrogen bonds.

3.5. Implications of Cellulose Pyrolysis Kinetics

Kinetic parameters of cellulose pyrolysis have been typically obtained using thermogravimetric analysis (TGA) by monitoring the mass change as a function of time or temperature, However, the apparent activation energies measured by TGA resulted in a wide range from 11 kcal mol^{-1} to 67 kcal mol^{-1}.[23] It is important to understand the apparent activation energies in the context of mechanistic modeling. Burnham et al.[68] reported the apparent activation energy of cellulose pyrolysis to be approximately 47 kcal mol^{-1} using a sigmoidal reaction model in a comprehensive review of mechanistic calculations. Agarwal et al.[69] pointed out that the apparent activation energies must fall in the range of 45–48 kcal mol^{-1}, corresponding to the plausible pre-exponentials in the range from 10^{-13} to 10^{-14} s^{-1}. Our two-chain model gives a slightly higher activation energy (E_a = 50.8 kcal mol^{-1}) than the experimental 45–48 kcal mol^{-1} range. However, this increase in the activation energy is compensated by over an order of magnitude higher in the pre-exponential factor caused by the entropic contributions (A = 4.3 x 10^{-12} s^{-1}).

Dauenhauer et al.[70, 71] have identified two distinct regimes for cellulose fast pyrolysis based on millisecond scale kinetic experiments. Their later work[29, 72] postulated that the mechanisms for the two kinetic regimes are different: the high-temperature (> 467 °C) regime follows a mid-chain activation pathway whereas the low-temperature (< 467 °C) regime follows an end-chain scission mechanism catalyzed by intersheet hydrogen bonds connecting to a neighboring sheet, giving a transition state of a lower activation energy of 29.5 kcal mol^{-1}. Since cellulose sheets are in a higher density state and a lower entropic state at lower temperatures before phase transition,[67, 73] intersheet hydrogen bonds are stronger under these conditions, further supporting the validity of the intersheet catalytic mechanism.

Our study, however, focuses on the high-temperature cellulose pyrolysis mechanism at 500 °C after phase transition. The mechanism is expected to be drastically different from the low-temperature (< 467 °C) catalytic mechanism reported by Dauenhauer et al. Under high temperature (> 467 °C) conditions, cellulose sheets take a lower density state, and the intersheet hydrogen bonds are weaken and not expected to play a significant role. Our temperature range of interest also falls into the low-temperature (< 900 K) cellulose

pyrolysis regime studied by Padmanathan and Mushrif[73], where the enthalpic contribution is expected to dominate. However, the gradual disruption of the hydrogen bonding network and gain of conformational flexibility in hydroxymethyl group orientation suggested in their work are consistent with our DFT findings, where intramolecular hydrogen bonds are found to be weaken in our two-chain model and the flexibility of hydroxymethyl group leads to ring puckering and more energetically favorable conformations prior to cellulose activation.

The unique contribution of our work is the discovery of a transition state enabled by intrachain hydrogen bonds for the high-temperature mid-chain scission mechanism. This new transition state gives a lower activation barrier (50.8 kcal mol^{-1}) than the ones obtained by other DFT studies in the literature (e.g., 58.0 kcal mol^{-1} [15] and 59.1 kcal mol^{-1} [29]) by more than 7.2 kcal mol^{-1} and is closer to the reported experimental range (45–48 kcal mol^{-1})[69].

4. Conclusions

Cellulose activation and subsequent LG formation *via* concerted glycosidic bond cleavage was studied using DFT. The roles of local environment near the reaction center and noncovalent interactions between cellulose chains are illuminated. The following conclusions can be drawn from our study:

1. Cellulose assumes ring puckering before its activation. Our calculations suggest that syn-$^1C_4$ is the most stable preactivated cellulose conformation to undergo subsequent activation *via* glycosidic bond cleavage.
2. A new cellulose activation mechanism incorporating intramolecular hydroxyl-activated glycosidic bond cleavage is discovered. The activation energy is predicted as 50.8 kcal mol^{-1} based on the two-chain model accounting for interchain hydrogen bonds. This value presents a closer agreement with the experimentally measured apparent activation energies of 45–48 kcal mol^{-1} range compared to existing predictions in the literature. Cellulose activation primarily takes place between the interior units of the

611 top (reactive) chain and is more energetically challenging than LG formation, which is predicted to have
612 an activation energy of 40.9 kcal mol^{-1}.
613 3. The presence of intramolecular and interchain hydrogen bonds achieves very tight binding between
614 cellulose chains and significantly alters the atomic and electronic structure of the chains, resulting in
615 both steric inhibition during cellulose activation and catalytic acceleration during LG formation by the
616 adjoining chain during cellulose pyrolysis.

617 The molecular-level understanding of cellulose pyrolysis behavior presented in this work not only provides
618 updated parameters for constructing kinetic models for cellulose pyrolysis but also establishes a framework
619 for studying noncovalent interactions between major biomass constituents, such as cellulose and lignin,
620 during the pyrolysis of actual biomass or biomass mixtures.

Supporting Information

The Supporting Information is available free of charge.

Cartesian coordinates, electronic energies, enthalpies, and free energies for all structures, details of the ring puckering pathways; and concerted reaction pathways in the anti conformation, details of the structural characterization as well as the methodology for chain models (PDF)

Declaration of interests

The authors declare no competing financial interest.

Acknowledgements

This work was supported by the National Science Foundation (NSF) (Award Number CBET-1847289). This work was completed in part with resources provided by the University of Massachusetts' Green High Performance Computing Cluster (GHPCC).

References

(1) Dhyani, V.; Bhaskar, T. A Comprehensive Review on the Pyrolysis of Lignocellulosic Biomass. *Renewable Energy* **2018**, *129*, 695-716.

(2) Amenaghawon, A. N.; Anyalewechi, C. L.; Okieimen, C. O.; Kusuma, H. S. Biomass Pyrolysis Technologies for Value-Added Products: A State-of-the-Art Review. *Environ Dev Sustain* **2021**, *23*, 14324-14378.

(3) Wang, G.; Dai, Y.; Yang, H.; Xiong, Q.; Wang, K.; Zhou, J.; Li, Y.; Wang, S. A Review of Recent Advances in Biomass Pyrolysis. *Energy Fuels* **2020**, *34*, 15557-15578.

(4) Brown, R. C.; Stevens, C. V. *Thermochemical Processing of Biomass : Conversion into Fuels, Chemicals and Power*; John Wiley & Sons, Incorporated, Hoboken, UNITED KINGDOM, 2011.

(5) Bridgwater, A. V. Review of Fast Pyrolysis of Biomass and Product Upgrading. *Biomass Bioenergy* **2012**, *38*, 68-94.

(6) Huber, G. W.; Iborra, S.; Corma, A. Synthesis of Transportation Fuels from Biomass: Chemistry, Catalysts, and Engineering. *Chem. Rev.* **2006**, *106*, 4044-4098.

(7) Mettler, M. S.; Vlachos, D. G.; Dauenhauer, P. J. Top Ten Fundamental Challenges of Biomass Pyrolysis for Biofuels. *Energy Environ. Sci.* **2012**, *5*, 7797-7809.

(8) Kostetskyy, P.; Broadbelt, L. J. Progress in Modeling of Biomass Fast Pyrolysis: A Review. *Energy Fuels* **2020**, *34*, 15195-15216.

(9) Mettler, M. S.; Mushrif, S. H.; Paulsen, A. D.; Javadekar, A. D.; Vlachos, D. G.; Dauenhauer, P. J. Revealing Pyrolysis Chemistry for Biofuels Production: Conversion of Cellulose to Furans and Small Oxygenates. *Energy Environ. Sci.* **2012**, *5*, 5414-5424.

(10) Patwardhan, P. R.; Satrio, J. A.; Brown, R. C.; Shanks, B. H. Product Distribution from Fast Pyrolysis of Glucose-Based Carbohydrates. *J. Anal. Appl. Pyrolysis* **2009**, *86*, 323-330.

(11) Lu, Q.; Yang, X.-c.; Dong, C.-q.; Zhang, Z.-f.; Zhang, X.-m.; Zhu, X.-f. Influence of Pyrolysis Temperature and Time on the Cellulose Fast Pyrolysis Products: Analytical Py-Gc/Ms Study. *J. Anal. Appl. Pyrolysis* **2011**, *92*, 430-438.

(12) Maduskar, S.; Maliekkal, V.; Neurock, M.; Dauenhauer, P. J. On the Yield of Levoglucosan from Cellulose Pyrolysis. *ACS Sustainable Chem. Eng.* **2018**, *6*, 7017-7025.

(13) Hu, B.; Zhang, B.; Xie, W.-l.; Jiang, X.-y.; Liu, J.; Lu, Q. Recent Progress in Quantum Chemistry Modeling on the Pyrolysis Mechanisms of Lignocellulosic Biomass. *Energy Fuels* **2020**, *34*, 10384-10440.

(14) Mayes, H. B.; Broadbelt, L. J. Unraveling the Reactions That Unravel Cellulose. *J. Phys. Chem. A* **2012**, *116*, 7098-7106.

(15) Hosoya, T.; Sakaki, S. Levoglucosan Formation from Crystalline Cellulose: Importance of a Hydrogen Bonding Network in the Reaction. *ChemSusChem* **2013**, *6*, 2356-2368.
(16) Dai, G.; Wang, K.; Wang, G.; Wang, S. Initial Pyrolysis Mechanism of Cellulose Revealed by in-Situ Drift Analysis and Theoretical Calculation. *Combust. Flame* **2019**, *208*, 273-280.
(17) Zhang, X.; Yang, W.; Dong, C. Levoglucosan Formation Mechanisms During Cellulose Pyrolysis. *J. Anal. Appl. Pyrolysis* **2013**, *104*, 19-27.
(18) Yang, X.; Fu, Z.; Han, D.; Zhao, Y.; Li, R.; Wu, Y. Unveiling the Pyrolysis Mechanisms of Cellulose: Experimental and Theoretical Studies. *Renewable Energy* **2020**, *147*, 1120-1130.
(19) Dai, G.; Zhu, Y.; Yang, J.; Pan, Y.; Wang, G.; Reubroycharoen, P.; Wang, S. Mechanism Study on the Pyrolysis of the Typical Ether Linkages in Biomass. *Fuel* **2019**, *249*, 146-153.
(20) Zhang, X.; Li, J.; Yang, W.; Blasiak, W. Formation Mechanism of Levoglucosan and Formaldehyde During Cellulose Pyrolysis. *Energy Fuels* **2011**, *25*, 3739-3746.
(21) Bradbury, A. G. W.; Sakai, Y.; Shafizadeh, F. A Kinetic Model for Pyrolysis of Cellulose. *J. Appl. Polym. Sci.* **1979**, *23*, 3271-3280.
(22) Lu, Q.; Hu, B.; Zhang, Z.-x.; Wu, Y.-t.; Cui, M.-s.; Liu, D.-j.; Dong, C.-q.; Yang, Y.-p. Mechanism of Cellulose Fast Pyrolysis: The Role of Characteristic Chain Ends and Dehydrated Units. *Combust. Flame* **2018**, *198*, 267-277.
(23) Lin, Y.-C.; Cho, J.; Tompsett, G. A.; Westmoreland, P. R.; Huber, G. W. Kinetics and Mechanism of Cellulose Pyrolysis. *J. Phys. Chem. C* **2009**, *113*, 20097-20107.
(24) Hutchinson, C. P.; Lee, Y. J. Evaluation of Primary Reaction Pathways in Thin-Film Pyrolysis of Glucose Using 13c Labeling and Real-Time Monitoring. *ACS Sustainable Chem. Eng.* **2017**, *5*, 8796-8803.
(25) Nallar, M.; Wong, H.-W. Enhanced Levoglucosan Yields from the Copyrolysis of Cellulose and High-Density Polyethylene. *ACS Sustainable Chem. Eng.* **2019**, *7*, 9480-9488.
(26) Proano-Aviles, J.; Lindstrom, J. K.; Johnston, P. A.; Brown, R. C. Heat and Mass Transfer Effects in a Furnace-Based Micropyrolyzer. *Energy Technol.* **2017**, *5*, 189-195.
(27) Assary, R. S.; Curtiss, L. A. Thermochemistry and Reaction Barriers for the Formation of Levoglucosenone from Cellobiose. *ChemCatChem* **2012**, *4*, 200-205.
(28) Zhang, Y.; Liu, C.; Chen, X. Unveiling the Initial Pyrolytic Mechanisms of Cellulose by Dft Study. *J. Anal. Appl. Pyrolysis* **2015**, *113*, 621-629.
(29) Maliekkal, V.; Maduskar, S.; Saxon, D. J.; Nasiri, M.; Reineke, T. M.; Neurock, M.; Dauenhauer, P. Activation of Cellulose Via Cooperative Hydroxyl-Catalyzed Transglycosylation of Glycosidic Bonds. *ACS Catal.* **2019**, *9*, 1943-1955.
(30) Hosoya, T.; Nakao, Y.; Sato, H.; Kawamoto, H.; Sakaki, S. Thermal Degradation of Methyl B-D-Glucoside. A Theoretical Study of Plausible Reaction Mechanisms. *J. Org. Chem.* **2009**, *74*, 6891-6894.

(31) Seshadri, V.; Westmoreland, P. R. Concerted Reactions and Mechanism of Glucose Pyrolysis and Implications for Cellulose Kinetics. *J. Phys. Chem. A* **2012**, *116*, 11997-12013.

(32) Frisch, M. J.; Trucks, G. W.; Schlegel, H. B.; Scuseria, G. E.; Robb, M. A.; Cheeseman, J. R.; Scalmani, G.; Barone, V.; Petersson, G. A.; Nakatsuji, H.; et al. *Gaussian 16*, Rev. C.01; Gaussian, Inc.: Wallingford, CT, 2016.

(33) Zhao, Y.; Truhlar, D. G. The M06 Suite of Density Functionals for Main Group Thermochemistry, Thermochemical Kinetics, Noncovalent Interactions, Excited States, and Transition Elements: Two New Functionals and Systematic Testing of Four M06-Class Functionals and 12 Other Functionals. *Theor. Chem. Acc.* **2008**, *120*, 215-241.

(34) Mayes, H. B.; Broadbelt, L. J.; Beckham, G. T. How Sugars Pucker: Electronic Structure Calculations Map the Kinetic Landscape of Five Biologically Paramount Monosaccharides and Their Implications for Enzymatic Catalysis. *J. Am. Chem. Soc.* **2014**, *136*, 1008-1022.

(35) Easton, M. W.; Nash, J. J.; Kenttämaa, H. I. Dehydration Pathways for Glucose and Cellobiose During Fast Pyrolysis. *J. Phys. Chem. A* **2018**, *122*, 8071-8085.

(36) Breneman, C. M.; Wiberg, K. B. Determining Atom-Centered Monopoles from Molecular Electrostatic Potentials. The Need for High Sampling Density in Formamide Conformational Analysis. *J. Comput. Chem.* **1990**, *11*, 361-373.

(37) Schlegel, H. B. Optimization of Equilibrium Geometries and Transition Structures. *J. Comput. Chem.* **1982**, *3*, 214-218.

(38) Peng, C.; Bernhard Schlegel, H. Combining Synchronous Transit and Quasi-Newton Methods to Find Transition States. *Isr. J. Chem.* **1993**, *33*, 449-454.

(39) Hratchian, H. P.; Schlegel, H. B. Accurate Reaction Paths Using a Hessian Based Predictor–Corrector Integrator. *J. Chem. Phys.* **2004**, *120*, 9918-9924.

(40) Hratchian, H. P.; Schlegel, H. B. Chapter 10 - Finding Minima, Transition States, and Following Reaction Pathways on Ab Initio Potential Energy Surfaces. In *Theory and Applications of Computational Chemistry*, Dykstra, C. E., Frenking, G., Kim, K. S., Scuseria, G. E. Eds.; Elsevier, Amsterdam, 2005; pp 195-249.

(41) Hratchian, H. P.; Schlegel, H. B. Using Hessian Updating to Increase the Efficiency of a Hessian Based Predictor-Corrector Reaction Path Following Method. *J. Chem. Theory Comput.* **2005**, *1*, 61-69.

(42) Zhao, Y.; Truhlar, D. G. Computational Characterization and Modeling of Buckyball Tweezers: Density Functional Study of Concave–Convex Π···Π Interactions. *Phys. Chem. Chem. Phys.* **2008**, *10*, 2813-2818.

(43) Ribeiro, R. F.; Marenich, A. V.; Cramer, C. J.; Truhlar, D. G. Use of Solution-Phase Vibrational Frequencies in Continuum Models for the Free Energy of Solvation. *J. Phys. Chem. B* **2011**, *115*, 14556-14562.
(44) Ayala, P. Y.; Schlegel, H. B. Identification and Treatment of Internal Rotation in Normal Mode Vibrational Analysis. *J. Chem. Phys.* **1998**, *108*, 2314-2325.
(45) Pfaendtner, J.; Yu, X.; Broadbelt, L. J. The 1-D Hindered Rotor Approximation. *Theor. Chem. Acc.* **2007**, *118*, 881.
(46) Grimme, S. Supramolecular Binding Thermodynamics by Dispersion-Corrected Density Functional Theory. *Chem. Eur. J.* **2012**, *18*, 9955-9964.
(47) Chai, J.-D.; Head-Gordon, M. Long-Range Corrected Hybrid Density Functionals with Damped Atom–Atom Dispersion Corrections. *Phys. Chem. Chem. Phys.* **2008**, *10*, 6615-6620.
(48) Eyring, H. The Activated Complex in Chemical Reactions. *J. Chem. Phys.* **1935**, *3*, 107-115.
(49) Evans, M. G.; Polanyi, M. Some Applications of the Transition State Method to the Calculation of Reaction Velocities, Especially in Solution. *Trans. Faraday Society* **1935**, *31*, 875-894.
(50) Wang, S.; Dai, G.; Yang, H.; Luo, Z. Lignocellulosic Biomass Pyrolysis Mechanism: A State-of-the-Art Review. *Prog. Energy Combust. Sci.* **2017**, *62*, 33-86.
(51) Dapprich, S.; Komáromi, I.; Byun, K. S.; Morokuma, K.; Frisch, M. J. A New Oniom Implementation in Gaussian98. Part I. The Calculation of Energies, Gradients, Vibrational Frequencies and Electric Field Derivatives1dedicated to Professor Keiji Morokuma in Celebration of His 65th Birthday.1. *J. Mol. Struct.: THEOCHEM* **1999**, *461-462*, 1-21.
(52) Vreven, T.; Byun, K. S.; Komáromi, I.; Dapprich, S.; Montgomery, J. A.; Morokuma, K.; Frisch, M. J. Combining Quantum Mechanics Methods with Molecular Mechanics Methods in Oniom. *J. Chem. Theory Comput.* **2006**, *2*, 815-826.
(53) Clemente, F. R.; Vreven, T.; Frisch, M. J. Getting the Most out of Oniom: Guidelines and Pitfalls. In *Quantum Biochemistry*, Matta, C. F. Ed.; Wiley-VCH, Weinheim, 2010; pp 61-83.
(54) Burns, L. A.; Mayagoitia, Á. V.-.; Sumpter, B. G.; Sherrill, C. D. Density-Functional Approaches to Noncovalent Interactions: A Comparison of Dispersion Corrections (Dft-D), Exchange-Hole Dipole Moment (Xdm) Theory, and Specialized Functionals. *J. Chem. Phys.* **2011**, *134*, 084107.
(55) Grimme, S.; Antony, J.; Ehrlich, S.; Krieg, H. A Consistent and Accurate Ab Initio Parametrization of Density Functional Dispersion Correction (Dft-D) for the 94 Elements H-Pu. *J. Chem. Phys.* **2010**, *132*, 154104.
(56) Goerigk, L.; Hansen, A.; Bauer, C.; Ehrlich, S.; Najibi, A.; Grimme, S. A Look at the Density Functional Theory Zoo with the Advanced Gmtkn55 Database for General Main Group Thermochemistry, Kinetics and Noncovalent Interactions. *Phys. Chem. Chem. Phys.* **2017**, *19*, 32184-32215.

(57) Schwarz, J. C. P. Rules for Conformation Nomenclature for Five- and Six-Membered Rings in Monosaccharides and Their Derivatives. *J. Chem. Soc., Chem. Commun.* **1973**, 14, 505-508.
(58) Stoddart, J. F. *Stereochemistry of Carbohydrates*; Wiley-Interscience, New York, 1971.
(59) Nishiyama, Y.; Langan, P.; Chanzy, H. Crystal Structure and Hydrogen-Bonding System in Cellulose Iβ from Synchrotron X-Ray and Neutron Fiber Diffraction. *J. Am. Chem. Soc.* **2002**, *124*, 9074-9082.
(60) Nishiyama, Y.; Sugiyama, J.; Chanzy, H.; Langan, P. Crystal Structure and Hydrogen Bonding System in Cellulose Iα from Synchrotron X-Ray and Neutron Fiber Diffraction. *J. Am. Chem. Soc.* **2003**, *125*, 14300-14306.
(61) Jeffrey, G. A. *An Introduction to Hydrogen Bonding*; Oxford University Press, New York, 1997.
(62) Kimura, F.; Oshima, W.; Matsumoto, H.; Uekusa, H.; Aburaya, K.; Maeyama, M.; Kimura, T. Single Crystal Structure Analysis Via Magnetically Oriented Microcrystal Arrays. *CrystEngComm* **2014**, *16*, 6630-6634.
(63) Matthews, J. F.; Bergenstråhle, M.; Beckham, G. T.; Himmel, M. E.; Nimlos, M. R.; Brady, J. W.; Crowley, M. F. High-Temperature Behavior of Cellulose I. *J. Phys. Chem. B* **2011**, *115*, 2155-2166.
(64) Ardèvol, A.; Biarnés, X.; Planas, A.; Rovira, C. The Conformational Free-Energy Landscape of B-D-Mannopyranose: Evidence for a 1s5 → B2,5 → Os2 Catalytic Itinerary in B-Mannosidases. *J. Am. Chem. Soc.* **2010**, *132*, 16058-16065.
(65) Uriarte, I.; Écija, P.; Lozada-Garcia, R.; Çarçabal, P.; Cocinero, E. J. Investigating the Conformation of the Bridged Monosaccharide Levoglucosan. *ChemPhysChem* **2018**, *19*, 766-773.
(66) Smrcok, L.; Sladkovicova, M.; Langer, V.; Wilson, C. C.; Koos, M. On Hydrogen Bonding in 1,6-Anhydro-[Beta]-D-Glucopyranose (Levoglucosan): X-Ray and Neutron Diffraction and Dft Study. *Acta Crystallogr., Sect. B: Struct. Sci., Cryst. Eng. Mater.* **2006**, *62*, 912-918.
(67) Agarwal, V.; Huber, G. W.; Jr., W. C. C.; Auerbach, S. M. Simulating Infrared Spectra and Hydrogen Bonding in Cellulose Iβ at Elevated Temperatures. *J. Chem. Phys.* **2011**, *135*, 134506.
(68) Burnham, A. K.; Zhou, X.; Broadbelt, L. J. Critical Review of the Global Chemical Kinetics of Cellulose Thermal Decomposition. *Energy Fuels* **2015**, *29*, 2906-2918.
(69) Agarwal, V.; Dauenhauer, P. J.; Huber, G. W.; Auerbach, S. M. Ab Initio Dynamics of Cellulose Pyrolysis: Nascent Decomposition Pathways at 327 and 600 °C. *J. Am. Chem. Soc.* **2012**, *134*, 14958-14972.
(70) Krumm, C.; Pfaendtner, J.; Dauenhauer, P. J. Millisecond Pulsed Films Unify the Mechanisms of Cellulose Fragmentation. *Chem. Mater.* **2016**, *28*, 3108-3114.
(71) Zhu, C.; Krumm, C.; Facas, G. G.; Neurock, M.; Dauenhauer, P. J. Energetics of Cellulose and Cyclodextrin Glycosidic Bond Cleavage. *Reaction Chemistry & Engineering* **2017**, *2*, 201-214.
(72) Maliekkal, V.; Dauenhauer, P. J.; Neurock, M. Glycosidic C–O Bond Activation in Cellulose Pyrolysis: Alpha Versus Beta and Condensed Phase Hydroxyl-Catalytic Scission. *ACS Catal.* **2020**, *10*, 8454-8464.

(73) Padmanathan, A. M. D.; Mushrif, S. H. Pyrolytic Activation of Cellulose: Energetics and Condensed Phase Effects. *Reaction Chemistry & Engineering* **2022**, *7*, 1136-1149.

803 **TOC Graphic**

804